



Roger, I., and [Symes, M. D.](#) (2016) First row transition metal catalysts for solar-driven water oxidation produced by electrodeposition. *[Journal of Materials Chemistry A](#)*, 4(18), pp. 6724-6741. (doi:[10.1039/C5TA09423B](#))

This is the author's final accepted version.

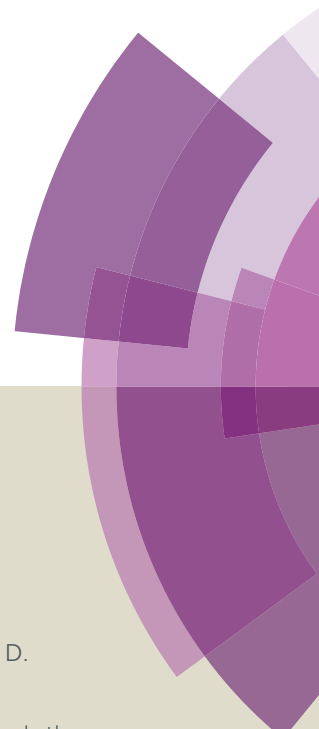
There may be differences between this version and the published version. You are advised to consult the publisher's version if you wish to cite from it.

<http://eprints.gla.ac.uk/114759/>

Deposited on: 14 January 2016

Journal of Materials Chemistry A

Accepted Manuscript



This article can be cited before page numbers have been issued, to do this please use: I. Roger and M. D. Symes, *J. Mater. Chem. A*, 2016, DOI: 10.1039/C5TA09423B.



This is an *Accepted Manuscript*, which has been through the Royal Society of Chemistry peer review process and has been accepted for publication.

Accepted Manuscripts are published online shortly after acceptance, before technical editing, formatting and proof reading. Using this free service, authors can make their results available to the community, in citable form, before we publish the edited article. We will replace this *Accepted Manuscript* with the edited and formatted *Advance Article* as soon as it is available.

You can find more information about *Accepted Manuscripts* in the [Information for Authors](#).

Please note that technical editing may introduce minor changes to the text and/or graphics, which may alter content. The journal's standard [Terms & Conditions](#) and the [Ethical guidelines](#) still apply. In no event shall the Royal Society of Chemistry be held responsible for any errors or omissions in this *Accepted Manuscript* or any consequences arising from the use of any information it contains.



Journal Name

ARTICLE

First Row Transition Metal Catalysts for Solar-Driven Water Oxidation Produced by Electrodeposition

Isolda Roger and Mark D. Symes*

Received 00th January 20xx,
Accepted 00th January 20xx

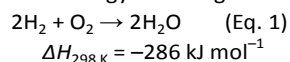
DOI: 10.1039/x0xx00000x

www.rsc.org/

As our reliance on renewable energy resources increases, so will our need to store this energy in the form of chemical fuels to iron-out peaks and troughs in supply. Sunlight, the most plentiful source of renewable energy, is especially problematic in this regard as it is so diffuse. One way to convert solar irradiation to fuels effectively would be to develop large surface area photo-electrochemical devices that could use sunlight directly to split water into H₂ and O₂. However, in order to be feasible, such an approach requires that these devices (and their components) are extremely cheap. In this review, we will discuss catalysts for the water oxidation half-reaction of electrochemical water splitting that can be produced by electrodeposition (a technique well suited to large-scale, low-cost applications), and that are based on the comparatively plentiful and inexpensive first row transition metals. Special attention will be paid to the electrodeposition conditions used in the various examples given, and structure-function relationships for electrochemical water oxidation for the materials produced by these techniques will be elucidated.

1. Introduction

There is an enormous (and growing) literature dedicated to electrochemical and photo-electrochemical water splitting for the production of hydrogen (and other potential fuels).¹⁻³ This is in large part due the fact that the products of water splitting (H₂ and O₂) make an excellent fuel-oxidant combination that re-forms water as the energy-releasing reaction occurs:

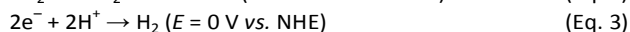
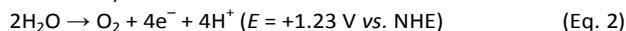


Hence a cycle that uses sustainably-sourced energy to split water into hydrogen and oxygen provides a way of generating a chemical fuel (H₂) that re-forms the substrate from which it was derived upon combustion: a highly attractive prospect from an environmental point of view. Accordingly, electrochemical water splitting has been proposed as a way of converting renewably-generated electricity (which tends to be prone to periods of surplus and deficiency in supply) into hydrogen, which could be stored for later use (for example when the renewable resource is temporarily unavailable, as with a solar panel at night).^{4,5} Such an approach would help to iron-out peaks and troughs in supply and would also provide a means by which electricity could be converted into a practical and tractable fuel.

In order for the economics of any such system to be viable on a large scale, the cost of the energy used to split the water (286 kJ mol⁻¹ according to Equation 1) and the cost of the water splitting devices themselves must be kept to a

minimum. An especially attractive route to achieving the former aim is to use sunlight as the energy source.⁶ Sunlight is widely distributed across the globe, it is a sustainable energy source, and it is free. It is also true that it is a rather diffuse resource, which (as we shall see) is somewhat of a double-edged sword. The latter aim (keeping the cost of the devices low) is one of the main reasons why Earth-abundant catalysts are so highly desired in this context.

The two half-reactions of water splitting (under standard conditions) can be written as:



where NHE is the Normal Hydrogen Electrode. Hence any electrochemical or photo-electrochemical device for water splitting will require an anode (at which to perform oxidation of water or hydroxide to produce O₂) and a cathode (at which to reduce protons or water to produce H₂). These reactions are more energetically challenging to perform than the 1.23 V suggested by Equations 2 and 3 (overpotential is required) and finding suitable catalysts for these reactions is therefore essential. Of the two reactions, water oxidation is generally held to be the more challenging, as four electrons must transfer per molecule of O₂ produced. Hence interest in developing new water oxidation catalysts has been particularly intense.

In a typical water electrolyser (which operates simply by using an electrical input to drive Equations 2 and 3), current densities (equating to amounts of oxygen and hydrogen produced per unit area of electrode per unit time) tend to be on the order of hundreds to thousands of mA per square centimetre.⁷ Such high current densities are not hard to achieve when working with a steady supply of power at a set

WestCHEM, School of Chemistry, University of Glasgow, University Avenue, Glasgow, G12 8QQ, UK. * Email: mark.symes@glasgow.ac.uk

voltage, but they are much harder to obtain when working with diffuse sunlight as the sole energy source. Indeed, the solar flux severely limits the expected maximum photocurrent density that could be produced by a solar-powered water splitting platform,⁸ and a benchmark current density of 10 mA cm⁻² can be taken as that expected for a 10% efficient solar-to-fuels conversion device operating under 1 Sun illumination.^{9,10} These comparatively low current densities may appear to be a wholly negative aspect of solar-driven hydrogen production, but on the flip-side low current density also means that the water oxidation and proton reduction catalysts do not need to demonstrate high efficacy at the current densities found in the typical water electrolyzers discussed above, but only in the low tens of mA cm⁻² range. Suitable catalysts for solar-driven water splitting must, however, be cheap and abundant as they will be required to cover large surface areas in order to produce useful amounts of hydrogen on practical timescales. Hence there is a great need to develop catalysts for solar-powered water splitting that use cheap and abundant elements and that can perform the oxygen evolution reaction (OER, Equation 2) and the hydrogen evolution reaction (HER, Equation 3) effectively at current densities of ~10 mA cm⁻². In this review, we will examine electrodeposited catalysts for the OER that are based on the first row transition metals Mn, Fe, Co, Ni and Cu. These elements are generally classed as “non-precious metals” and are both more plentiful and less expensive than elements such as Ru, Rh, Pt and Ir (and hence suitable for coating a large surface area solar-to-hydrogen array). Table 1 gives current prices, reserves and annual productions for these metals, as reported by the US Geological Survey.¹¹ Hence it is evident that there is considerable variation in price and abundance even amongst the so-called “earth-abundant” elements, but that the platinum group metals (and silver, to a lesser extent) are significantly more expensive and rare.

Table 1: Prices, reserves and global production of the metals discussed in this review and selected precious metals.

Metal	Price (\$/tonne)	Known global reserves (Thousand metric tonnes)	World production in 2014 (Thousand metric tonnes)
Mn	1,630	570,000	18,000
Fe	53	87,000,000	3,200,000
Co	26,000	7,200	112
Ni	9,500	81,000	2,400
Cu	4,900	700,000	18,700
Ru	1,350,000	-	-
Rh	23,800,000	-	-
Pd	17,700,000	-	0.19
Ag	464,000	530	26
PMGs ^a	-	66	-

^a PMGs are the platinum group metals and include Pt, Pd, Ir, Os, Ru and Rh.

2. Electrodeposition as a Synthetic Strategy

Electrodeposition as a strategy by which to access materials for water oxidation has several key advantages. Firstly, the

technique is scalable to large surface areas and is therefore amenable to mass production.¹² This renders the production of extended solar-to-hydrogen arrays technologically feasible. Secondly, electrodeposition can be performed both in the laboratory and industrially with comparatively cheap equipment and straightforward procedures – this should help to keep the costs of such arrays to a minimum.¹³ Moreover, electrodeposition offers great scope for control over the catalyst deposition process. For example, as it is very easy to control the amount of charge passed during a deposition, the amount of material deposited (and hence the film thickness) can be tuned, allowing films of only a few nanometres to be deposited. Such control can be achieved through altering the time of deposition, the current at which deposition is performed (whether steady or varying according to a pre-defined schedule), or through a combination of these. The control over film thickness this allows is especially important in instances where solar irradiation is to be used to drive water oxidation: thin catalyst films ensure that the amount of light reaching the underlying photo-active substrate is not significantly attenuated by scattering or absorbance in the catalyst layer.

The oxidation state of the metal(s) in electrodeposited films, and the morphology of the deposited material can be controlled through the potential that is applied. In trivial terms, this means that more oxidising potentials give rise to more oxidised deposits (favouring therefore more oxidised phases of the deposited materials), but it is also possible to deposit metal oxide films through ramping the potential or by cycling the potential. These latter approaches enable strategies whereby a particular polymorph of the material is deposited at a lower potential and is then oxidised *in situ* to give a more highly oxidised version of the oxide that retains certain morphological features characteristic of the lower oxide (and where deposition at higher potentials from the outset without ramping from a lower voltage would give a different morphology in the final oxide that might be less active). This strategy has been used extensively for the deposition of manganese oxides that are active for water oxidation (see Section 5).

A combination of photo- and electrodeposition is also possible (photo-electrochemical deposition), whereby materials are formed on the electrode through the simultaneous application of a potential and irradiation of the semiconductor electrode surface, which acts to generate an additional bias favouring metal oxide deposition. As we shall see in this review, photo-electrodeposition often gives rise to more uniform deposited films than can be produced through electrodeposition alone (see Section 8). Moreover, we shall also see in this review examples where the initial electrodeposition is *reductive*, first producing a metal layer on the electrode, which is subsequently converted to the oxide electrochemically or through chemical oxidation (see especially methods for the production of mixed NiFe oxides in Section 7). Thus electrodeposition offers great scope for altering the morphology of the films produced through the alteration of potential during deposition.

Electrodeposition also presents opportunities for diversity in terms of the choice of deposition solution (also termed the “deposition bath”). This includes the pH of the bath, the temperature of the bath, the use of additives, and the concentration of the soluble precursors. The nature of these precursors themselves is a further variable that can be tuned to great advantage. Simple metal salts are the most frequently used precursors, but in the following we will also discuss several examples where more sophisticated metal-ligand complexes have been employed, often leading to films with exceptional uniformity. Finally, catalysts that can be prepared by electrodeposition also offer a potential route to “self-repair” under the conditions of subsequent catalysis. It is a crucial requirement for any durable and practical device that catalytic performance does not deteriorate significantly with operation over extended time periods, and hence an ability for the catalysts to re-generate during operation is a major boon. Hence through a deliberate combination of the features mentioned above, films with variable morphologies, structures, oxidation states and hence electrochemical properties can be produced by electrodeposition.^{14,15} We shall begin our review of the literature with an example of a self-repairing catalyst, and one that has played a significant role in galvanising this field in recent years.

3. Electrodeposited Catalysts for Water Oxidation Based on Cobalt

In 2008, Nocera and co-workers reported a cobalt oxy-hydroxide-based catalyst for the oxygen evolution reaction (OER) that self-assembled on the anode when solutions of cobalt(II) salts in neutral phosphate buffer were subjected to a modest anodic bias.^{16,17} The composition of the catalyst (nicknamed “CoPi”) was determined by a range of structural and analytical techniques, and was postulated to be based on incomplete Co-oxo cubanes, as illustrated in Figure 1.^{18,19} The catalyst was composed solely of “earth-abundant” elements (Co, O, P and cations from the electrolyte such as K⁺). Selective oxidation of water to produce oxygen was also shown to be possible with this catalyst from phosphate-buffered seawater and from buffered (but otherwise untreated) river water, which bodes well for the development of low-cost devices for sustainable water splitting using this material.²⁰ A proposed mechanism for the electrodeposition and subsequent turn-over of CoPi is shown in Figure 1. Initially, soluble Co(II) ions are oxidised to Co(III) at the anode, leading to the formation of insoluble Co(III)-oxides (possibly with phosphates associated with the Co(III) centres) as a deposit on the surface of the anode. As the anodic potential is increased, some of these Co(III) centres undergo a further oxidation to Co(IV).²¹ This is the active state of the catalyst, which oxidises water to O₂ and protons. As this happens, the Co(IV) centres are reduced back to the Co(II) oxidation state, and these Co(II) ions may dissolve into solution and then re-deposit as Co(III)-oxides. It is this dissolution and re-deposition under anodic bias (effectively a continuous dissolution and electrodeposition cycle) which is postulated to be the mechanism of catalyst re-assembly and repair.²² Hence the

catalyst maintains activity over an extended period of time through functional, rather than structural, stability.

The same group also demonstrated that other anions apart from phosphate could be used to support this electrodeposition reaction and subsequent water oxidation. In particular, sodium borate (at pH 9) was shown to be at least as effective as phosphate buffer,²³ and often superior catalytic activity was observed in borate solution (see Table 2). This was suggested to be linked to the differing intermediate-range structures of the phosphate and borate-derived catalysts: catalyst films electrodeposited in borate electrolyte were generally composed of coherent domains in which cobaltate clusters of between 3 and 4 nm in size with up to three layers formed, whereas films electrodeposited from phosphate electrolyte exhibited smaller clusters that were not coherently stacked.²⁴

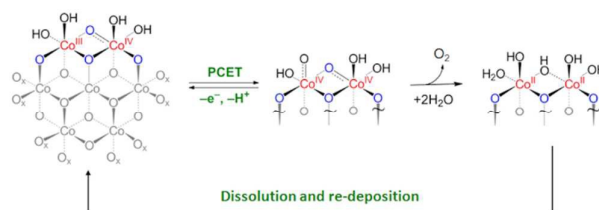


Fig. 1 The proposed structure and mechanism of operation of the CoPi water oxidation catalyst. In the key step, the mixed Co(III)/Co(IV) resting state of the catalyst undergoes a proton-coupled electron transfer (PCET) event, to give the active Co(IV) oxide state. This reacts with water to liberate O₂, with the Co(IV) centres being reduced to Co(II) in the process. Dissolution and oxidative re-deposition of these Co(II) ions regenerates the catalyst in its resting state, constituting a self-repair mechanism.

Table 2: Key data for selected electrodeposited Co-oxide catalysts discussed in Section 3, with values for IrO₂ and RuO₂ provided for reference.²⁵

Reference	Electrolyte salt	pH	Overpotential at 1 mA cm ⁻² (mV)	Tafel Slope (mV decade ⁻¹)
16	KPi ^a	7	410	60
20	KBi ^b / seawater	9.2	530	75
23	KBi	9.2	390	60
26	KPi	7	540	-
27	KF	3.5	<500	120
28	NaOH	13	320	54
30	KOH	14	300	49 ^c
31	NaOH	14	440	60
32	KOH	14	320	47
36	NaOH	14	~400	60-70
37	KBi	9.2	450	60
38	KBi	9.2	600 ^d	60
40	KBi	9.2	500 ^e	60
IrO ₂	KOH	13	320	55
IrO ₂	HClO ₄	1	290	45
RuO ₂	KOH	13	320	80
RuO ₂	HClO ₄	1	280	50

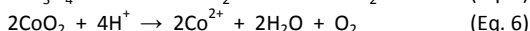
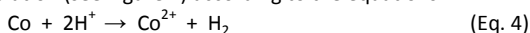
^a KPi = potassium phosphate. ^b KBi = potassium borate. ^c Crystalline. ^d Gives 5 mA cm⁻². ^e Gives 4 mA cm⁻².

Remaining in near-neutral electrolytes, Cobo *et al.* have reported a catalyst system able to mediate both proton reduction to H₂ and water oxidation to O₂ using electrodeposited Co-oxides.²⁶ CoPi-like deposits were grown under anodic bias from solutions of cobalt(II) nitrate on FTO substrates, and found to deliver similar metrics for water oxidation in phosphate buffer at pH 7 to those reported

previously by Nocera.¹⁶ However, when these catalysts were poised cathodically the electrodeposited Co-oxides did not dissolve, but rather they were reduced on the electrode to cobalt metal with a thin overlayer of a cobalt-oxy-phosphate material. This proved to be a reasonable hydrogen evolution catalyst in buffered neutral solutions, giving a current density of 1 mA cm^{-2} for hydrogen production at around 400 mV overpotential.

The above examples employed neutral and near-neutral pH regimes, in part because such electrolytes are compatible with many of the more common light-harvesting semiconductors that could be used in monolithic solar-to hydrogen devices. However, cobalt oxy-hydroxides that are competent for water oxidation can also be electrodeposited at much lower pH. Stahl and co-workers have demonstrated this by electrodepositing cobalt oxides on the anode from solutions of potassium fluoride containing CoSO_4 at pH 3.5.²⁷ The films produced in this way were found to be robust, and supported electrochemical water oxidation at a current density of 1 mA cm^{-2} at overpotentials of less than 500 mV. Some of the same authors subsequently expanded on these results and investigated electrocatalytic water oxidation with cobalt in a range of buffers across the pH range 0-14. These studies showed that Co-oxide films electrodeposited from solutions containing 1-20 mM Co(II) are heterogeneous, oligomeric, layered double-hydroxide materials. These films mediate water oxidation to O_2 at pHs above 3.5, but at lower pHs these films dissolve to give soluble Co(II) species which mediate water oxidation to H_2O_2 .²⁸

Bloor *et al.* subsequently showed that both a Co-oxide water oxidation catalyst and a Co-metal based proton reduction catalyst could be electrodeposited simultaneously from the same electrolyte bath (0.2 M $\text{Co}_2(\text{PO}_4)_3$ at pH 1.6) under an applied bias, and that these catalysts were functionally stable for the two half reactions of water splitting for as long as the potential difference across the cell was at least 2 V.²⁹ Moreover, the authors were able to demonstrate that these electrodeposited catalysts were metastable at pH < 2, and that if the circuit was opened the films re-dissolved into the electrolyte bath with concomitant O_2 and H_2 evolution (see Figure 2) according to the equations:



Hence, although the Faradaic yield for O_2 and H_2 production during electrolysis (when a potential was applied) was below unity, full Faradaic efficiency for the production of both gases was obtained upon complete dissolution of the films. This work served to highlight the ability of first row transition metals to mediate heterogeneous electrolytic water splitting in acidic media by exploiting, rather than trying to avoid, the natural propensity of electrodeposits of these metals to dissolve at low pH. Co-oxide catalysts can, therefore, mediate the OER over the pH range 2 - 14 and could possibly have activity at pHs below 2 if large enough

voltages and high enough concentrations of Co are used.

Fig. 2 Graph showing how oxygen continued to evolve from electrodeposited Co-oxide films after the cessation of electrolysis at pH 1.6. The blue line shows when a potential of 2.2 V (two-electrode configuration) was applied (see scale on right hand axis). The red line and circles indicate the amount of O_2 detected in the headspace of the electrolysis cell (left hand axis), whilst the black line shows the total amount of oxygen expected at any given time, based on the assumption that O_2 was only produced during electrolysis. Hence it is evident that O_2 is released both during electrolysis and when no potential is applied. This figure was adapted from Bloor *et al.* (reference 29).

At the other end of the pH scale, Switzer and co-workers electrodeposited films of Co_3O_4 by oxidation of solutions containing Co(II) tartrate at pH 14.³⁰ Another important distinction between this work and the examples already mentioned is that the electrodepositions in this case were carried out at elevated temperatures. These conditions were found to have significant ramifications for the morphology of the deposits thus formed: films deposited between 50 and 90 °C were amorphous (and readily exfoliated from the electrode), but films deposited from refluxing solution at 103 °C were crystalline and adhered strongly to the substrate. The crystalline films were found to have the normal spinel structure, and exhibited Tafel slopes of 49 mV/decade and an exchange current density of $2.0 \times 10^{-10} \text{ A cm}^{-2}$, whereas the amorphous films had Tafel slopes of 36 mV/decade and exchange current densities two orders of magnitude lower than the crystalline films. Both types of film, it was claimed, showed superior activity for the OER than CoPi, although it should be noted that the pH regimes employed here and in Nocera's studies above are rather different.

An alternative electrodeposition strategy was reported recently by Mavr , Limoges and co-workers using carbon-coated metal nanoparticles as the metal source.³¹ These metal nanoparticles have the advantage that they are magnetic and can thus be induced to cluster on an electrode surface without the application of any potential bias simply by judicious positioning of a magnet (Figure 3). Subsequent anodization of these magnetically-clustered nanoparticles led to their conversion into an amorphous metal oxide film, which in the case of cobalt was found to deliver current densities in excess of 10 mA cm^{-2} at less than 800 mV overpotential. Compared to formation of Co-oxide films by electrodeposition from solutions containing Co(II) salts, the use of carbon-coated cobalt nanoparticles has the advantage that it significantly improves the rate of catalyst deposition whilst also allowing an element of pre-positioning of material prior to electrodeposition through the use of the magnetic manipulations.

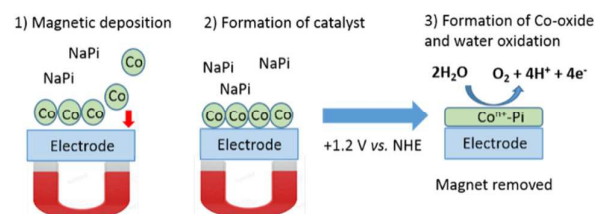
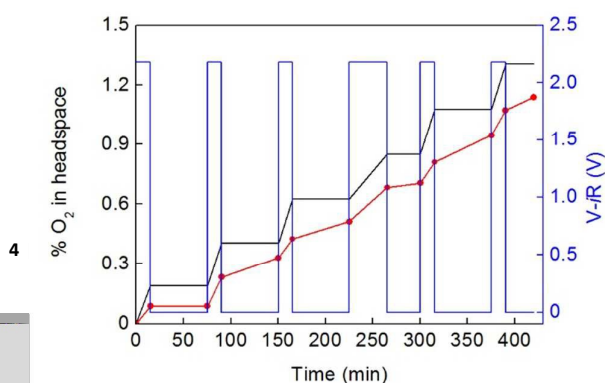


Fig. 3 Schematic depiction of the magnetically-assisted electrodeposition of Co-oxides reported by Mavr  and Limoges. NaPi = sodium phosphate buffer.

An electrodeposited bifunctional catalyst for the OER and HER from alkaline solutions was published recently by Sun and co-workers.³²



Initially a cobalt-phosphorus film was reductively electrodeposited onto a copper substrate. The films thus produced were competent hydrogen evolution electrocatalysts, but of more relevance to the current discussion is their use as catalysts of the OER. By poisoning these films anodically in 1 M KOH, current densities for the OER of 10 mA cm^{-2} could be obtained at 350 mV overpotential. X-ray photon spectroscopy (XPS) analysis of the film showed high levels of Co, P and O in the films. Co 2p peaks corresponding to Co-oxides were evident (e.g. peaks for Co_3O_4 at 780.7 and 796.3 eV), but signals for metallic cobalt (778.0 and 793.0) were also well-resolved. Hence these films appear to be a mixture of Co-oxide phases with pockets of more reduced cobalt species.

Co-oxide films for water oxidation have also been deposited from solutions of more sophisticated cobalt salts and complexes. Stracke and Finke have shown that solutions containing the polyoxoanion $[\text{Co}_4(\text{H}_2\text{O})_2(\text{PW}_9\text{O}_{34})_2]^{10-}$ at pH 8 can be used to electrodeposit a heterogeneous Co-oxide film that is competent for water oxidation, and that this effect manifests at polyoxoanion concentrations as low as $2.5 \mu\text{M}$.^{33,34} This work was originally intended to highlight some of the hazards associated with distinguishing between homogeneous and heterogeneous catalysis under the conditions probed, but the electrodeposition of Co-oxide films using polyoxometalates as templates has since been exploited by others in deliberate attempts to produce water oxidation catalysts. For example, Lai *et al.* used Co-containing polyoxotitanates as precursors for the subsequent electrosynthesis of Co-oxide phases within a titania matrix under anodic bias.³⁵ Meanwhile, Liu *et al.* have demonstrated the utility of the niobium Linqvist ion $[\text{Nb}_6\text{O}_{19}]^{8-}$ as a stabilizing additive during the electrodeposition of Co(II) and Ni(II) salts as their respective oxy-hydroxides.³⁶ On the basis of Raman spectroscopy, a mechanism of film formation involving the electrostatic stabilization of $\text{Co}(\text{OH})_2$ or $\text{Ni}(\text{OH})_2$ nanoparticles by the $[\text{Nb}_6\text{O}_{19}]^{8-}$ anion was proposed, resulting in films containing Co and Ni oxy-hydroxide nanoparticles of between 30 and 40 nm in diameter.

Metal-ligand coordination complexes of cobalt have been used as precursors for the electrodeposition of Co-oxide films by Du and co-workers, who have explored both Co-salen³⁷ and Co cobaloxime complexes³⁸ for this purpose (salen = N,N'-ethylenebis(salicylimine)). Films derived from Co-salen precursors displayed onset of catalytic water oxidation at ~ 350 mV and both films gave very high Faradaic efficiencies for the production of O_2 . Ullman *et al.* have reported catalytic water oxidation at appreciable levels by heterogeneous cobalt oxides deposited from Co(II) impurities present in solutions of cobalt-oxo cubane coordination complexes.³⁹ In a similar vein, Bonke *et al.* have recently used a series of cobalt amino-polycarboxylate complexes as precursors from which to deposit Co-oxide water oxidation catalysts.⁴⁰ The use of such precursors was held to allow control over the deposition rate and morphology of the films thus produced and hence to enable the production of thin catalyst films on the conductive substrate. In the case of a photoelectrode generated using a cobalt-nitritriacetate complex as the Co source, this strategy resulted in a film that absorbed only 10% of the incident light whilst still generating >80% of the water oxidation current produced by a film derived from the simple $[\text{Co}(\text{OH}_2)_6]^{2+}$ cation (whose transmission was only 40% at those same

wavelengths). Hence the authors reasoned that using amino-polycarboxylate complexes to electrodeposit Co-oxide water oxidizing catalysts would be of utility in the fabrication of combined light-harvesting and water-oxidizing electrodes.

4. Electrodeposited Catalysts for Water Oxidation Based on Nickel

Soon after reporting the CoPi water oxidation catalyst, Nocera described its nickel analogue (electrodeposited from borate solutions at pH 9), so-called "NiBi".⁴¹ The procedure for producing this catalyst was again very simple (electrodeposition onto the anode was induced by applying +1.2 V vs. NHE in a 100 mM sodium borate solution containing 1 mM Ni^{2+}) and, as with CoPi, amorphous metal oxy-hydroxide deposits were obtained. In the case of NiBi, a Tafel slope of 58 mv/decade and an overpotential requirement of ~ 420 mV to achieve 1 mA cm^{-2} were initially reported. These values were subsequently both revised downwards after it was noted that anodization of these films caused an improvement in catalysis of the OER, with slopes of 30 mV/decade manifesting after sufficient anodic polarization.⁴² It was postulated that non-anodized films were less active due to a requirement for a large reorganization energy associated with a Jahn-Teller distortion in the Ni(III) resting state of the catalyst. The necessary anodization step, and the rest of the proposed mechanism for the operation of this catalyst, is shown in Figure 4. Hence the borate-bound Ni(III) resting state gives rise to a nickel oxy-hydroxide material which mediates water oxidation through a series of proton-coupled-electron transfers. Further evidence for this cycle was found through correlated coulometric and X-ray absorption near-edge structure spectra, which suggested that Ni centres in activated films were in an average oxidation state of +3.6 (compared to an average oxidation state of +3 in unactivated films). This in turn suggested that a significant proportion of the Ni centres in activated films were in the Ni(IV) oxidation state (cf. the mechanism suggested for CoPi, see Figure 1).⁴³

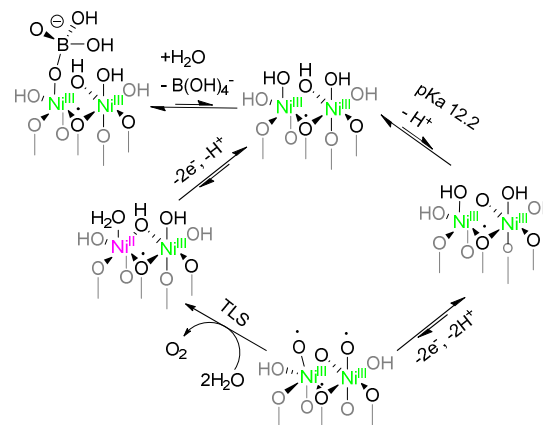


Fig. 4 The proposed structure and mechanism of operation of the NiBi water oxidation catalyst, showing the initial activation step (with loss of borate) and the various subsequent postulated oxidation states of the catalyst during turnover. TLS = turnover-limiting step.

Furthermore, these structural studies revealed that activated catalyst films were composed of bis-oxo / hydroxo-bridged Ni

ARTICLE

Journal Name

centres arranged in sheets of edge-sharing NiO₆ octahedra. These findings were supported by independent structural analysis of these films by Dau and co-workers, who noted the strong similarities between the atomic structure of NiBi and its CoPi cousin.⁴⁴ Nocera's early work in this area also established the optimum pH range over which electrodeposited nickel oxides are effective catalysts of the OER. Above pH ~8, NiBi outperforms CoPi and is the more active water oxidation catalyst. However, below pH 6, the performance of NiBi falls off rapidly, with current densities on the order of only 1 μA cm⁻² being obtained at 300 mV overpotential at pH 6.⁴²

Numerous alternative strategies have been used to obtain NiBi-type catalysts on a number of different substrates. For example, Wiley and co-workers electrodeposited nickel from solutions of NiCl₂ onto copper nanowires to give Ni-coated structures, which displayed 95% Faradaic efficiency for electrochemical O₂ production (see Table 3).⁴⁵ An alternative route to highly-structured electrodeposited NiBi-type materials has been reported by Hu and co-workers.⁴⁶ In this work, composite Ni-SiO₂ films were electrodeposited from a solution containing nickel sulfate, boric acid and tetramethoxysilane in ethanol/water at -1.1 V vs. Ag/AgCl. The SiO₂ template was then etched by subjecting the composite electrodes to cyclic voltammetry in 1 M KOH. As the SiO₂ dissolved with each successive cycle, the peak associated with the Ni(III)/Ni(II) redox wave steadily grew, which the authors attributed to an increase in the number of electrochemically active Ni centres (as these centres became exposed as a result of the etching of the insulating SiO₂ matrix). The resulting structures were highly porous, with a consequent increase in surface area. Thus, current densities for the OER in 1 M KOH for these films (based on geometric surface area) are around ten times higher at +0.8 V vs. Ag/AgCl than they are for a control Ni film obtained by the same methods but from a deposition bath containing no tetramethoxysilane.

Bifunctional catalysts able to perform both the OER and HER have been reported using electrodeposited nickel oxides. Both Wu⁴⁷ and Du⁴⁸ used cathodic potentials and borate solutions containing Ni(II) ions to deposit catalyst films competent for the HER in potassium borate solution. Subsequent application of anodic bias in both cases converted the deposited materials into competent water oxidation catalysts, with electrochemical and structural properties broadly in agreement with Nocera's NiBi films.

Table 3: Key data for selected electrodeposited Ni-oxide catalysts discussed in Section 4.

Reference	Electrolyte salt	pH	Overpotential at 1 mA cm ⁻² (mV)	Tafel Slope (mV decade ⁻¹)
42	KBi ^a	9.2	380	30
45	KBi	9.2	610 ^b	-
46	KBi	9.1	450	72
46	KOH	14	320 ^c	90 and 200 ^d
48	KBi	9.2	~400	137
49	NaBi ^e	9.2	~500	105
50	NaBi	9.2	600 ^f	100-110

^a KBi = potassium borate. ^b Gives 0.8 mA cm⁻². ^c Gives 10 mA cm⁻². ^d Two regions in Tafel slope. ^e NaBi = sodium borate. ^f Catalyst derived from the tacn precursor.

As with the cobalt oxides (Section 3), molecular precursors have been used in the electrodeposition of nickel oxide films for the OER. Spiccia and co-workers have applied this approach using the Ni complexes shown in Figure 5. In the case of [Ni(en)₃]Cl₂ (en = 1,2-diaminoethane), electrodeposition was carried out at +1.1 V vs. Ag/AgCl from sodium borate buffer containing the metal complex at 1 mM concentration.⁴⁹ Films of NiBi were electrodeposited under the same conditions from simple inorganic Ni(II) salts for comparison. Subsequent water oxidation assays showed that films derived from [Ni(en)₃]Cl₂ out-performed films derived from inorganic Ni(II) salts under the same conditions. By X-ray absorption spectroscopy (XAS), the authors determined that the films formed from the simple salts and [Ni(en)₃]Cl₂ alike were all predominantly γ-NiOOH. However, the morphologies of the films differed, with those electrodeposited from [Ni(en)₃]Cl₂ being more homogenous and having higher electroactive surface areas (as determined by capacitance measurements). In contrast, when the same authors electrodeposited Ni-oxide films from the three macrocyclic Ni(II) complexes shown in Figure 5 (Ni(tacn) and Ni(cyclen) complexes, where tacn = 1,4,7 triazacyclononane and cyclen = 1,4,8,11 tetraazacyclotetradecane), the effectiveness of each of these films for the OER in the dark was essentially the same as that delivered by a NiBi film electrodeposited from a solution containing a simple inorganic salt (although a modest improvement in current density did manifest under illumination).⁵⁰ Clearly then, more investigation is required in order to ascertain the true benefits of this approach.

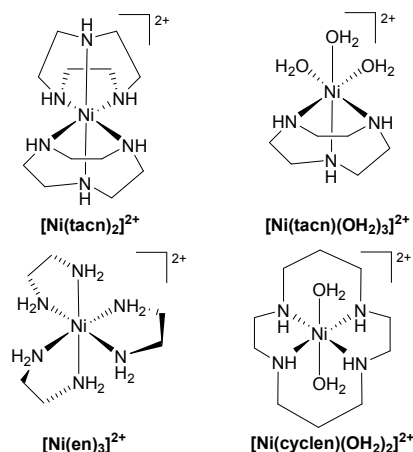


Fig. 5 The Ni complexes discussed in the main text that have been used as precursors in the electrodeposition of Ni-oxides for electrocatalytic water oxidation. The abbreviations used in the figure are as follows: tacn = 1,4,7 triazacyclononane en = 1,2-diaminoethane, cyclen = 1,4,8,11 tetraazacyclotetradecane.

The final example of Ni-oxide electrodeposition for the OER that we shall consider is of interest on account of the fact that nickel was not deliberately added to the electrolyte baths during deposition at all, but was instead found to be present in ostensibly "clean" borate, phosphate and carbonate buffers as a trace impurity.⁵¹ Accordingly, when bare FTO, ITO, Pt or carbon electrodes were poised anodically in these buffers at basic pH, current densities were observed to rise dramatically over the course of several hours (see Figure 6), reaching current densities of over 1 mA cm⁻² at

overpotentials of 400 mV. The cause of this behaviour was determined by XPS to be the electrodeposition of Ni-oxides on the anode. By careful and repeated washing of the electrolytes with an ion-chelating resin, the authors were able to remove sufficient Ni from these electrolyte solutions to prevent significant current density increases from occurring upon anodic polarization. This study highlights an age-old problem in catalysis (namely, what is the true catalyst in any given situation?^{52,53}) and will require any new putative water oxidation catalysts that display similar OER metrics to prove that trace metal impurities in the electrolytes are not the root cause of the observed activity.

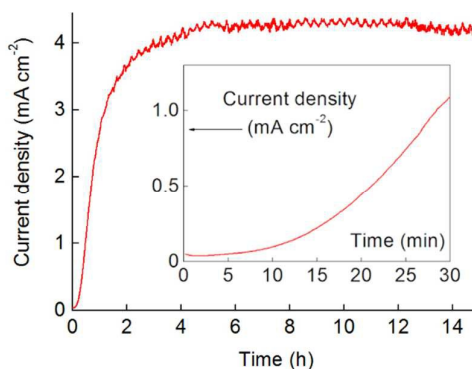


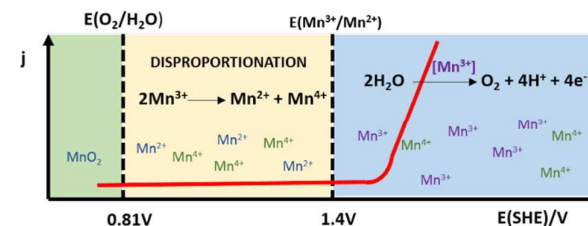
Fig. 6 Bulk electrolysis at +1.4 V vs. NHE in ostensibly pure potassium borate buffer (pH 9.2) that was subsequently shown to contain traces of Ni^{2+} . The current density rose steadily for around 5 hours before reaching a plateau. Inset: an expansion of the first 30 minutes of electrolysis. Figure adapted from reference 51.

5. Electrodeposited Catalysts for Water Oxidation Based on Manganese

Mn-oxo cubanes are found in Nature in photosystem II, which is responsible for mediating water oxidation in the leaves of plants.⁵⁴ Manganese oxides have also been known to effect electrocatalytic water oxidation for some time.^{55,56} Over the last few years, however, there has been a resurgence of interest in these materials, with a new emphasis on mild conditions and improved current densities. In 2010, Gorlin and Jaramillo reported a bifunctional Mn-based catalyst, able to catalyse both water oxidation and its reverse (the ORR) in 0.1 M KOH solution.⁵⁷ The catalyst material was electrodeposited onto glassy carbon anodes, before calcination at 480 °C in air for 10 hours. Following this treatment, the Mn-oxo film (which X-ray diffraction and scanning electron microscopy suggested was nano-structured $\alpha\text{-Mn}_2\text{O}_3$) was found to have bifunctional catalytic activity for the OER and ORR comparable to that of precious metals. XPS analysis of the active Mn oxide catalyst revealed the Mn centres in the film to be in the 3+ oxidation state. In a subsequent publication, the authors examined the structure of these electrodeposited Mn-oxide films during catalysis of the OER using *in situ* XAS.⁵⁸ This showed that the films were highly porous and suggested that a mixture of two Mn-oxide phases existed under the highly oxidising conditions pertaining to the OER: a birnessite-type MnO_2 phase and a more reduced mixed-valence oxide, $\text{Mn}_3^{\text{II,III,III}}\text{O}_4$. The authors suggested that the more oxidised phase was significant for OER catalysis, but

urged further study of the structural parameters and surface conditions during turnover. Jaramillo and co-workers also assessed the photoactivity of films of MnO_2 electrodeposited at +1 V vs. Ag/AgCl from solutions containing 2 mM MnSO_4 , and determined that this material displays a modest increase in current density for the OER under illumination. Photo-induced current density enhancements of between 50 and 100 $\mu\text{A cm}^{-2}$ were obtained at anodic biases of between 1.6 and 1.7 V vs. RHE.⁵⁹

Some sense of the inherent limitations of such Mn-oxide catalysts was provided by Takashima *et al.* in 2012.⁶⁰ These authors noted that manganese oxides are efficient water oxidation catalysts under basic conditions, but that this activity drops off dramatically at neutral pH. Using spectroelectrochemical methods to monitor changes in the composition of Mn-oxide catalysts during electrocatalytic water oxidation, Takashima *et al.* found a remarkable fall in catalytic activity at pH values below 8 (see Table 4).⁶¹ Careful analysis of these results then led the authors to conclude that this drop-off in activity occurs at pH values where Mn^{3+} ions start to disproportionate into Mn^{2+} and Mn^{4+} , in the form of soluble Mn(II) salts and insoluble MnO_2 . Hence, the authors reasoned, in order to obtain sustained electrocatalytic water oxidation with Mn-oxides, the pH should be maintained well above



pH 8 (in practice, at pH 13 or above), at which pH the catalytically active Mn(III)-species are stabilised (see Figure 7).

Fig. 7 Illustration of the current density (j) vs. potential curve for MnO_2 at neutral pH according to Takashima *et al.* showing where disproportionation occurs.

Zaharieva, Dau and co-workers have tackled this issue head-on in their work studying water oxidation with electrodeposited Mn-oxides at pH 7.⁶² Starting from 0.5 mM solutions of Mn(II) acetate in 0.1 M acetate buffer (pH 6), the authors prepared two distinct types of manganese oxide films. The first class were deposited by bulk electrolysis at various fixed potentials over the range +0.95 to +2.15 V vs. NHE. All these films gave rather low activity for the OER, with the best of them delivering 0.2 mA cm^{-2} at 1.45 V vs. NHE. The second class of films were electrodeposited by a method in which the voltage was continuously varied between +2.15 and -0.75 V vs. NHE at a sweep rate of 100 mV per second. This technique produced films with much higher activity for the OER, now achieving around 1 mA cm^{-2} at 1.45 V vs. NHE. The structural differences between the two different classes of Mn-oxide were probed on the atomic scale by EXAFS (Extended X-Ray Absorption Fine Structure) spectroscopy. This revealed that the more active Mn-oxides had a high degree of disorder in their atomic structures, which the authors postulated might facilitate $\mu_2\text{-O(H)}$ bridging and terminal ligation of water and thus boost catalytic activity. The less active Mn-oxides, by contrast, were more akin to MnO_2 , which is both more ordered and more stable and thus more catalytically inert. A subsequent combined structural and computational study

ARTICLE

Journal Name

by some of the same authors suggested that the more active Mn-oxide films are formed of small planar Mn-oxo sheets that are linked together through various out-of-plane Mn atoms and groups of atoms. The authors also found that active films tended to have a greater number of coordinatively unsaturated and partially reduced Mn(III)O₅ moieties at the boundaries of the amorphous Mn-oxide network, which they speculated could act as hole traps and hence enable the oxidation of nearby water molecules under anodic bias. In contrast, Mn-oxide films that were inactive for the OER consisted of more extended Mn-oxo sheets comprised mainly of more oxidised, coordinatively saturated (and hence more inert) Mo(IV)O₆ blocks.⁶³

Ramires *et al.* have also investigated the structure-function relationships of the various Mn-oxides for catalysis of the OER.⁶⁴ These authors electrodeposited films onto FTO substrates galvanostatically, producing highly amorphous Mn-oxide films. These were then heat-treated at various temperatures in order to access different Mn-oxide phases, with α -Mn₂O₃ dominating after heating in air at 773 K and Mn₃O₄ dominating after heating under nitrogen at 873 K. Electrochemical analysis of the films for their efficacy for the OER suggested that the least active films were those composed of Mn₃O₄ (Mn₃^{II,III,III}O₄), whilst the most active were predominantly α -Mn₂O₃. Further analysis of these Mn-oxides after they had been used for the OER indicated that their surfaces were amorphous, with a variety of Mn-O bond lengths and a high concentration of oxygen point defects. Hence the authors concluded that the films with the highest activity for the OER were those containing a high proportion of Mn(III) centres in a structurally-disordered lattice. These findings seem broadly in agreement with those suggested to underlie high OER activity found by Dau and co-workers (above).^{62,63}

Electrodeposition followed by heat-treatment has also been employed by Zhou *et al.* who were able to demonstrate an improvement in catalysis of the OER by Mn-oxide films after heating.⁶⁵ Films were deposited galvanostatically and then heated in air at 50, 70, 90 or 120 °C. Films that had been heated displayed lower Tafel slopes and lower OER onset potentials in 1 M NaOH than films that had not been heated, with heating to 90 °C found to be the optimum (Table 4). A battery of analytical techniques (X-ray diffraction, scanning electron microscopy, energy dispersive X-ray spectroscopy (EDX), Fourier transform infrared spectroscopy and Raman spectroscopy) suggested that the main effect of heating was dehydration of the films, with no significant alterations to the microstructure or bulk composition being evident. XPS meanwhile, suggested the growth of reduced Mn species (either Mn(II) or Mn(III)) to a limited extent on the surface of films after heat treatment. The same team also investigated the electrodeposition of Mn-oxides for the OER from ionic liquid electrolytes at elevated temperatures.⁶⁶ Electrodepositions were conducted galvanostatically at 120 °C from an electrolyte consisting of 10 mM manganese(II) acetate in a 1:9 mixture of water and ethylammonium nitrate. Various film morphologies were obtained as a function of the acidity of the electrolyte, including nanowires, nanofibres and nanoparticles. Analysis of the chemical composition of the films revealed that those composed of Mn₃O₄ generally exhibited the lowest activity for the OER, whilst those containing

mixed Mn₂O₃ and birnessite phases had higher activity, again in agreement with the other studies on Mn-oxides mentioned above.

Table 4: Selected electrodeposited Mn-oxide catalysts discussed in Section 5.

Reference	Electrolyte salt	pH	Overpotential at 1 mA cm ⁻² (mV)	Tafel Slope (mV decade ⁻¹)
57	KOH	13	<300	-
60	Na ₂ SO ₄	6	720	-
62	KPi ^a	7	590	80
64	KOH	14	280 ^b	-
65	NaOH	14	300 ^c	114
67	KPi	6.8	480	120
69	KPi/KNO ₃	2.5	-	~650 ^d
69	KPi/KNO ₃	7	-	127
69	KPi/KNO ₃	12	-	60

^a KPi = potassium phosphate. ^b For α -Mn₂O₃. ^c Film heated to 90 °C. ^d Average.

Brudvig and co-workers have also examined the use of electrolytes containing additives for the electrodeposition of Mn-oxides for the OER. In their report,⁶⁷ the authors used aqueous deposition solutions containing various concentrations of MnSO₄ (1 – 100 mM) and one equivalent of the surfactant SDS (sodium dodecyl sulfate). Electrodeposition was then conducted onto FTO substrates by cyclic voltammetry as per the conditions of Zaharieva and Dau.⁶² Films were also deposited in the absence of SDS for comparison. Microstructure and elemental analyses revealed the electrodeposited materials to be mixed-phase manganese oxides, and suggested that films deposited with or without the addition of SDS to the electrolytes had very similar structures. However, a marked difference in electrochemical activity for the OER was observed: films deposited from SDS-containing electrolytes displayed overpotentials reduced by over 100 mV relative to films deposited in the absence of SDS.

The studies described above assess the ability of Mn-oxides to catalyse the OER under basic or neutral conditions. In contrast, Nocera and co-workers have recently studied the nucleation, growth and OER catalysis mechanism of electrodeposited Mn-oxides across the entire pH range 0-14.^{68,69} The catalytic films were deposited onto FTO substrates from electrolytes containing 0.5 mM MnCl₂ at pH 8. Detailed electrochemical analyses were then performed on these films in electrolytes at various pHs. At high pH, Tafel slopes for the OER on these Mn-oxide deposits were around 60 mV/decade and an inverse first order dependence on proton concentration was observed. This suggested a one-electron, one-proton proton-coupled-electron transfer equilibrium preceding a turnover-limiting chemical step under basic conditions. Conversely, catalysis of the OER under low pH conditions was independent of the proton concentration and the Tafel slopes were quasi-infinite, which the authors attributed to an initial chemical turnover-limiting step (believed in this case to correspond to disproportionation of surface Mn³⁺ centres at the catalyst surface). Intermediate Tafel slopes and proton-dependencies were observed at neutral pH. Therefore, the authors suggested that two competing mechanisms were in operation (one at low pH and the other at high pH), as shown in Figure 8. The presence of this alternative acid-regime mechanism thus explains why Mn-oxides can catalyse the OER at pH < 8, which would otherwise seem to be in contradiction of the

findings of Takashima *et al.* (see Figure 7 and references 60 and 61). The two mechanisms in Figure 8 also allow potential routes to catalyst self-healing to be identified (especially under acidic conditions), *via* continuous dissolution of kinetically-labile Mn(II) and re-deposition of MnO_x during turnover under anodic bias.

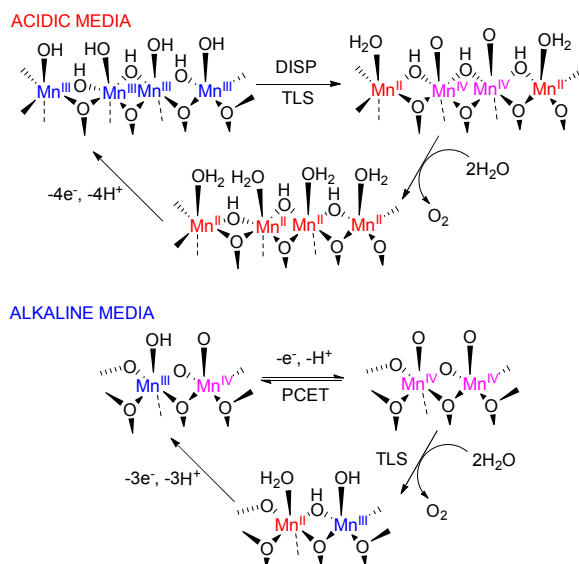


Fig. 8 Nocera's proposed mechanisms for the OER as mediated by manganese oxides under acidic and basic conditions. DISP = disproportionation.

6. Electrodeposited Catalysts for Water Oxidation Based on Copper and Iron

In recent years, electrodeposited copper oxides have also been suggested as catalysts for the OER. In 2013, Chen and Meyer noted during their investigation of water oxidation with soluble Cu(II) salts that electrodeposited films formed on the anode under certain conditions, and that these electrodeposits were competent for the OER.⁷⁰ Yu *et al.* have since expanded on this initial report and successfully electrodeposited copper oxide films (which when analysed proved to be composed chiefly of CuO) from borate buffer solutions containing 1 mM Cu(NO₃)₂.⁷¹ Tafel analysis of these films indicated a slope of around 90 mV/decade and an overpotential requirement for the OER of between 550 and 600 mV to achieve a current density of 1 mA cm⁻². This work also included a study of pH vs. current density at a fixed potential, demonstrating that Cu-oxide catalysts perform the OER more effectively at pH 9 and above, and that activity is much impaired below pH ~6.

Meanwhile, Cu-oxide films for the OER have also been prepared from Cu-containing metal-ligand complexes. This approach was first demonstrated by Du and co-workers, who used the Cu(II) complexes shown in Figure 9 to electrodeposit amorphous CuO films (as determined by XPS, EDX and XRD) on FTO electrodes. These films evinced high (>90%) Faradaic efficiencies for O₂ production under anodic bias at +1.41 V vs. NHE, and delivered current densities of 1 mA cm⁻² at 600 mV overpotential with a Tafel slope of 56 mV/decade at pH 9.2.⁷² A similar strategy has been followed by Fu and co-workers, who used the Cu(II) complex

[Cu(TEOA)(H₂O)₂][SO₄] as a source of copper for the electrodeposition of a copper oxide film, which also analysed as CuO (TEOA = triethanolamine).⁷³ Once again, near unity Faradaic efficiency was reported for oxygen production under anodic bias. However, in this case a Tafel slope of around 130 mV/decade was reported and more than 800 mV overpotential was required in order to obtain a current density of 1 mA cm⁻², in contrast to the results obtained by Du. Meanwhile, the Du group have shown that films electrodeposited from precursors similar to those in Figure 9 display bifunctional activity for both the OER and HER in basic solution, producing H₂ at a rate of 1 mA cm⁻² at 660 mV overpotential when poised cathodically and producing O₂ at a rate of 0.1 mA cm⁻² at 500 mV overpotential when used as an anode.⁷⁴

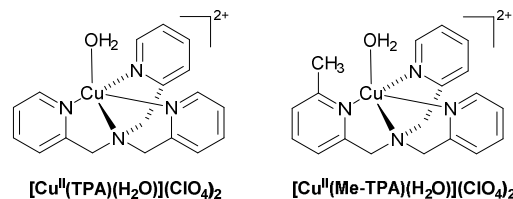


Fig. 9 The Cu complexes used by Du and co-workers as precursors in the electrodeposition of Cu-oxides for electrocatalytic water oxidation and proton reduction. TPA = tris(2-pyridylmethyl)amine.

Iron oxides have tended to lag behind the other late first row transition metals with respect to their use as electrodeposited catalysts for the OER, possibly on account of the low solubility of Fe(III) in neutral aqueous solution. Very recently, however, some reports of electrodeposited iron-oxide films as electrocatalysts for water oxidation have appeared. For example, iron-oxide films have been electrodeposited at neutral pH from solutions of FeSO₄ by cyclic voltammetry.⁷⁵ Only a few scans were found necessary in order to deposit films with a coverage of 10 nmol cm⁻², but films of this thickness still proved sufficiently active to deliver current densities of 1 mA cm⁻² at overpotentials of 530 mV (at neutral pH). The morphology of the deposits appeared to be iron-based polycrystalline particles of ~5 nm in size. Subsequent analysis of the films by XPS confirmed that Fe(III) was present on the electrode.⁷⁶

7. Electrodeposited Catalysts for Water Oxidation Based on Mixed-Metal Oxides

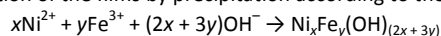
Whilst pure iron oxides are still emerging as potential water oxidation electrocatalysts, mixed-metal oxides containing iron and other late first row transition metals are much more established in this regard. Nearly 30 years ago, Corrigan showed that the presence of low levels of Fe (as low as 0.01%) in nickel oxide films had a significant effect on the kinetics of the OER.⁷⁷ This work has now taken on a new importance in the context of solar-to-fuels devices. Merrill and Dougherty electrodeposited mixtures of a wide range of commercially-available first row transition metal salts on Pt substrates and determined that oxides of Mn, Fe, Co, Ni, Cu, FeMn, CoFe, NiFe, NiCo, CuFe, and CuNi all enhanced electrochemical oxygen evolution activity relative to the bare Pt substrate.⁷⁸ Of these various active oxides, however, NiFe-oxides demonstrated the best overall catalytic performance for the OER at pH 14 (see

ARTICLE

Journal Name

Table 5). Tafel slopes as low as 15 mV/decade were reported and current densities of 500 mA cm⁻² were achieved at less than 300 mV overpotential. Morphologically, the optimal NiFe-oxide catalysts were determined to be highly disordered with XPS suggesting that NiFe₂O₄ was the dominant phase. Li *et al.* also examined electrodeposits of mixed Ni and Fe oxides for the OER under comparatively high current densities in 1 M NaOH.⁷⁹ The resulting NiFe-oxide films were able to perform the OER at a rate of 500 mA cm⁻² at only 265 mV overpotential, 70 mV less than for Ni-oxides without any iron. However, the authors noted that although small additions of Fe(II) to the predominantly Ni(II) deposition baths led to an enhancement of the OER, larger additions had the reverse effect, and in fact reduced the performance of the resulting mixed-metal electrodes below that exhibited by undoped Ni-oxides.

Lu and Zhao have studied nickel-iron electrodes for electrolytic water splitting across a wide range of current densities. In their report, high surface area macroporous nickel foam was used as the substrate.⁸⁰ Electrodeposits were then formed on this substrate by applying a reductive potential of -1 V vs. Ag/AgCl for five minutes from a bath containing 3 mM Ni(NO₃)₂ and 3 mM Fe(NO₃)₃ (see Figure 10). Hydroxide created at the surface of the cathode at these reductive potentials was invoked to explain the mechanism of formation of the films by precipitation according to the equation:



Deposition times were chosen so as to strike the best balance between depositing sufficient material on the electrode whilst still keeping the electrodeposited films thin enough so that charge transfer between the film and the nickel substrate was not inhibited. XPS and X-ray spectroscopy revealed that the optimal films were amorphous with a general formula of Ni₃Fe(OH)₉. The authors reported a Tafel slope for this material of 32 mV/decade for the OER at low current densities (1 – 10 mA cm⁻²) and stated that the overpotential requirements to reach current densities of 500 and 1000 mA cm⁻² (of relevance to electrolyzers that run off steady power inputs) were 240 and 270 mV respectively. This was reported to be the best catalyst for the OER in alkaline media yet discovered.

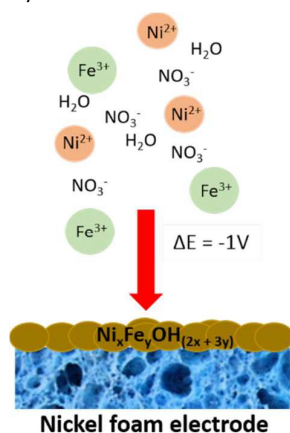


Fig. 10 The hydroxide-induced precipitation of mixed NiFe-oxides reported by Lu and Zhao.

Bell and co-workers have explored the role of Fe doping in Ni-oxides in depth from both an electrochemical and a structural perspective. Mixed Fe-Ni oxides of various compositions were prepared on gold

electrodes from solutions containing the corresponding ratios of FeSO₄ and NiSO₄.⁸¹ Once again, a cathodic galvanostatic method was used, in this case at a current density of 50 μA cm⁻² for 1125 seconds. Electrodeposited films containing 40% iron oxides gave current densities for the OER (at pH 13 and above) which were two orders of magnitude higher than films consisting solely of Ni-oxides and three orders of magnitude higher than films consisting solely of Fe-oxides. On the basis of cyclic voltammetry, it was suggested that increased Fe content in the films produced a progressive anodic shift in the position of the Ni(II)/Ni(III) redox wave (corresponding to the Ni(OH)₂/NiOOH couple at these high pHs), and hence caused the average oxidation state of the Ni at a given voltage to decrease as Fe content increased. Raman spectroscopy of these films evinced the presence of a structural unit akin to NiOOH in these mixed NiFe-oxides at potentials where the OER occurs and also showed that films exhibiting high activity for the OER tended to display a degree of disorder. The relative intensities of the two NiOOH bands (at 475 and 555 cm⁻¹) were also highly sensitive to the Fe content of the films. Hence the presence of Fe in these films dramatically affected the local environment around Ni, which in turn had a significant effect on the redox properties of these Ni centres.

Table 5: Key data for selected electrodeposited Mixed-metal-oxide catalysts discussed in this Section.

Reference	Oxides	pH	Overpotential at 1 mA cm ⁻² (mV)	Tafel Slope (mV decade ⁻¹)
78	Ni-Fe	14	30	15
79	Ni-Fe	14	~180	40
80	Ni-Fe	15	~120	32
81	Ni-Fe	13-15	300 ^d	40
87	Ni-Fe	14	210	31
88	Co-Fe	7	~300 ^b	30 ^b
89	Ni-Co	13	370	-
90	Ni-Mo	14	300 ^c	47
91	Co-Zn	13	430 ^d	83
92	Co-Cu	14	570 ^e	-
94	Ni-Co-Ce	14	250	~60
IrO ₂ ^f	KOH	13	320	55

^a Gives 10 mA cm⁻² when film composition is 40% Fe and 60% Ni. ^b When film composition is 55% Fe and 45% Co. ^c Gives 10 mA cm⁻². ^d Gives 2 mA cm⁻². ^e Gives 0.5 mA cm⁻². ^f From reference 25.

Further light has been shed on these results by the use of *in situ* High Energy Resolution Fluorescence Detection X-ray absorption spectroscopy (HERFD-XAS), which gave additional information on the local environment of the Ni and Fe centres in the material and how these changed with the changing potential.⁸² At potentials well below onset of the OER, Ni in Ni-oxide films was found to be present as α-Ni(OH)₂. In films containing Fe, however, the Ni was present as Ni(II)_{1-x}Fe(III)_x(OH)₂(SO₄)_{x/2}(H₂O)_y (a layered double hydroxide structure) at these same potentials. In these NiFe-oxide films, increasing the potential led to oxidation of the Ni(II) in the double hydroxide to Ni(III), whilst the Fe stayed as Fe(III). When the level of Fe doping in the films was less than 25%, this more oxidized catalyst could be described as γ-Ni_{1-x}Fe_xOOH. This supposition was supported by the Ni-O and Fe-O bond lengths in this material, which were both very similar to each other and also very similar to the Ni-O bond lengths in γ-NiOOH. Meanwhile, the Fe-O bond lengths in γ-

$\text{Ni}_{1-x}\text{Fe}_x\text{OOH}$ were around 6% shorter than in $\gamma\text{-FeOOH}$, an effect possibly induced by edge-sharing with surrounding $[\text{NiO}_6]$ octahedra. Hence the formula $\gamma\text{-Ni}_{1-x}\text{Fe}_x\text{OOH}$ reflects the substitution of Fe for Ni in a predominantly $\gamma\text{-NiOOH}$ lattice, with Fe(III) occupying the octahedral sites. When the level of Fe doping was above 25%, however, XAS suggested that extended phases of $\gamma\text{-FeOOH}$ formed, containing at most 3% Ni. By correlating these experimental results with computational analysis, the authors found that Fe(III) centres in $\gamma\text{-Ni}_{1-x}\text{Fe}_x\text{OOH}$ displayed a lower overpotential requirement for the OER than Ni(III) cations in either $\gamma\text{-Ni}_{1-x}\text{Fe}_x\text{OOH}$ or $\gamma\text{-NiOOH}$. Hence the significant (up to 500-fold) enhancement of the OER that is observed by doping of Ni-oxides with Fe was rationalized.

Boettcher and co-workers have also studied electrodeposited Fe-doped Ni-oxide water oxidation catalysts, but from the perspective of the iron manifesting as an impurity in the solutions from which these films are grown (see parallels with reference 51). The authors found that nickel oxy-hydroxides electrodeposited from rigorously Fe-free Ni salts and supporting electrolytes displayed much higher overpotential requirements for the OER in 1 M KOH than films deposited in the presence of trace iron.⁸³ For example, Ni-only films required an overpotential of about 470 mV to achieve a current density of 1 mA cm^{-2} but films containing adventitious traces of Fe delivered this current density at only 300 mV overpotential. Fe was clearly visible in the XPS spectra of these ostensibly pure Ni-oxides. By deliberately adding Fe to their deposition baths, the authors discovered that around 25% Fe doping produced the optimal performance for the OER, in good agreement with the work of Bell and co-workers discussed above.^{81,82} The authors proposed that enhancement of the OER could be brought about *via* a partial-charge transfer activation effect on Ni mediated by Fe. Noting that increasing the Fe content of NiFe-oxide films pushes the Ni(II)/Ni(III) couple to more anodic potentials (see similar arguments advanced by Bell, above), and that partial-charge transfer between Fe and $\text{Ni}^{3+/4+}$ was previously proposed by Corrigan,⁸⁴ the authors reasoned that adding Fe would therefore make it more difficult to oxidise the Ni(II) centres in the film and thus produce $\text{Ni}^{3+/4+}$ species with more oxidizing power and possibly enhanced OER activity. This work has been extended recently to include nickel oxide electrodeposits obtained from borate buffers at near neutral pH (similar conditions to those employed by Nocera and co-workers with their NiBi catalyst, see Section 4). Once again, the activity of the electrodeposits for the OER was significantly reduced (by a factor of 10) when electrolysis was conducted in rigorously Fe-free electrolytes and Fe was again observed by XPS on those films displaying enhanced activity. Indeed, Fe at levels as low as 1 ppm were found to lead to a significant enhancement in the OER activity, with consequent ramifications throughout the field.⁸⁵

Evidence for charge-transfer mechanisms producing superior OER activity in electrodeposited NiFe-oxides has also been found by Wang *et al.*⁸⁶ This team adapted a procedure originally reported by Corrigan⁷⁷ to deposit mixed nickel-iron oxides on carbon paper supports cathodically at pH 2. *In situ* and *ex situ* X-ray Absorption Near Edge Structure (XANES) techniques were then used to map the variations in electronic structure of the material during the OER. A significant degree of covalency was evident in the Fe-O bonds and the mean oxidant state of Ni was found to be +3.6 at anodic

potentials relevant to the OER (*cf.* Nocera's postulated mechanism for NiBi in Figure 4 and the associated discussion). The highly covalent Fe-O bonds in the otherwise $\gamma\text{-NiOOH}$ matrix were postulated to facilitate the transfer of electrons away from the Ni centres during anodic polarization, thus leading to higher catalytic activity in NiFe-oxide films than for films of pure nickel oxy-hydroxides. An Ni-Fe layered double hydroxide catalyst for water oxidation has been reported by Gong *et al.*, who electrodeposited these catalysts onto carbon nanotube supports.⁸⁷ The excellent electron transport properties of this substrate, coupled to the high intrinsic activity of crystalline Ni-Fe layered double hydroxides for the OER produced a system that out-performed IrO_2 as a water oxidation catalyst at basic pH (see Table 5).

In addition to their work with Fe-doped nickel oxides, Boettcher and co-workers have also demonstrated that Fe-doping of electrodeposited cobalt oxides can lead to significant enhancement of the OER from alkaline solution.⁸⁸ Indeed, incorporation of Fe into these films (whether by deliberate addition of Fe salts to the deposition baths, or as a result of Fe impurities being present in the cobalt salts used) was found to enhance the OER activity by up to two orders of magnitude when compared to similar studies conducted in rigorously Fe-free electrolytes. By a combination of techniques, the authors were able to assign the roles of Fe and Co in Fe-doped CoOOH ($\text{Co}_{1-x}\text{Fe}_x(\text{OOH})$) during catalysis of the OER. As with the nickel analogues, the position of the Co(II)/Co(III) redox wave moved to more anodic potentials with increasing Fe content in the films. The authors also noted that CoOOH is both a good electrical conductor and chemically stable to dissolution at the potentials where the OER occurs. Hence it was proposed that, although FeOOH is electrically insulating and unstable with respect to dissolution under conditions suitable for the OER in base, it had a higher intrinsic activity for the OER than did CoOOH . Hence the authors postulated that CoOOH acts as a conductive, chemically stable and porous host for the Fe centres, which in turn are the more active OER catalytic sites.

Lambert and co-workers recently communicated a $\text{Ni}_x\text{Co}_{3-x}\text{O}_4$ mixed oxide material with activity for both the OER and its reverse reaction, the reduction of oxygen to water (the "oxygen reduction reaction", or ORR).⁸⁹ Catalysts were electrodeposited galvanostatically from solutions containing cobalt(II) nitrate and nickel(II) nitrate in various ratios and then annealed at 573 K in air. Grazing angle X-ray diffraction spectra confirmed the formation of spinel phase NiCo_2O_4 -type materials in all cases. These films performed oxygen reduction in 0.1 M KOH, achieving -5 mA cm^{-2} at +0.7 V vs. RHE, but were also competent for the OER, delivering 10 mA cm^{-2} at +1.7 V vs. RHE. These are thus promising materials for use as reversible oxygen electrodes and have parallels with Gorlin and Jaramillo's Mn-based bifunctional oxygen reduction/water oxidation catalysts (see Section 5).

Meanwhile, Tian *et al.* have electrodeposited a NiMo alloys from solutions containing nickel(II)sulfate and sodium molybdate and showed that these materials function as both a hydrogen evolution catalysts and an oxygen evolution catalysts in basic media, although no detailed study of the structural or compositional changes in these materials on switching from the HER to the OER has yet been reported.⁹⁰

The use of electrodeposited binary zinc–cobalt layered double hydroxides as catalysts for the OER from 0.1 M KOH solution has been reported.⁹¹ The as-deposited films displayed a morphology in which “nanowalls” of material were oriented perpendicular to the plane of the underlying substrate, producing a high surface area electrode. Under anodic bias in 0.1 M KOH solution, these double layered hydroxide materials outperformed nickel, cobalt hydroxide and zinc hydroxide films, with the best performing of the Zn-Co materials giving over 20 mA cm⁻² for the OER at +1.8 V vs. RHE. Likewise, electrodeposited cobalt oxides doped with copper oxides are effective catalysts for the OER at pH 14.⁹² Using a unipolar pulse electrodeposition technique,⁹³ a CuO/Co₃O₄ material was obtained which exhibited an unusual morphology (described as resembling a sea-anemone). Modest increases in the current density for the OER were found when compared to pristine Co₃O₄ (see Table 5).

Finally, it is interesting to note the potential for high-throughput screening to identify new water oxidation catalysts, and the supporting role that independent electrochemical synthesis of potential targets can play. In this regard, Gregoire and co-workers used high-resolution inkjet printing to produce 5456 discrete oxide compositions containing the elements nickel, iron, cobalt and cerium.⁹⁴ From the various oxides produced, they identified Ce-rich materials as especially promising for the OER under conditions relevant to solar-driven water oxidation. They then used electrodeposition to synthesise one such candidate material, Ni_{0.2}Co_{0.3}Ce_{0.5}O_x, independently. This involved cathodic electrodeposition of material onto a gold electrode from a bath containing 20 mM nickel(II) nitrate, 30 mM cobalt(II) nitrate, 50 mM cerium(III) nitrate and 100 mM potassium nitrate. The resulting films produced current densities for the OER of 10 mA cm⁻² at 310 mV overpotential. The combination of high-throughput methods to identify new materials for the OER and electrodeposition to produce these materials at scale is tremendously powerful, and suggests one route by which this field may expand significantly in the near future. It is also of interest to note that the vast majority of the mixed metal catalysts discussed above have only been investigated under very basic conditions (pH 13 and above). Hence the field would benefit from a study of such catalysts at lower pH (especially under near-neutral conditions), which may be more suitable for interfacing these catalysts with semiconductors (as will be discussed in the next section).

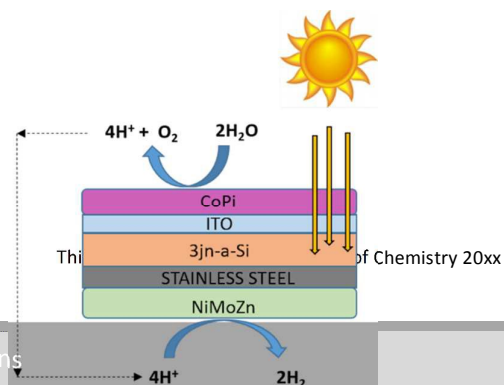
8. Electrodeposited Catalysts for Photo-Driven Water Oxidation

The ease with which Co-oxide can be induced to form has led many authors to view this as the catalyst of choice when decorating photoanodes for potential solar-driven water splitting. Importantly, Co-oxides are functional and stable at neutral pH, which is a key requirement for most of the better-developed semiconductor materials. One of the first such studies investigated the use of Nocera’s CoPi catalyst as a promoter of water photo-oxidation by hematite (α -Fe₂O₃).⁹⁵ Using CoPi, the water oxidation onset potential was reduced by more than 350 mV compared to unfunctionalized hematite, and subsequent optimization of the system allowed water oxidation to be conducted under irradiation

with a modest potential bias for over 6 hours.⁹⁶ Some of the same authors subsequently used a photo-assisted electrodeposition route to deposit CoPi on the surface of dendritic α -Fe₂O₃ meso-structures.⁹⁷ This route produced a 70 mV greater cathodic shift in the water oxidation onset potential than using electrodeposition alone, possibly as a result of the more uniform deposition of CoPi observed with the photo-assisted method. For photo-assisted electrodeposition, some of the requisite anodic bias was provided by irradiation of the hematite substrate (onto which the CoPi deposited), meaning that the biases required in order to produce Co-oxides on the anode were reduced by up to 800 mV in comparison to conventional electrodeposition under dark conditions.

Cobalt oxides have also been electrodeposited on other semiconducting substrates (see Table 6). Seabold and Choi electrodeposited a WO₃ semiconductor on a transparent fluorine-doped tin oxide (FTO) substrate and then electrodeposited a CoPi-like catalyst on top of this using Nocera’s reported conditions.⁹⁸ The activity of these electrodes was then compared to that of photoanodes prepared without any CoPi catalyst. Undecorated WO₃ films were observed to have a photocurrent to O₂ conversion efficiency of only 61%, with the remaining photo-generated holes producing peroxy species which degraded the performance of the photoanodes. However, those electrodes bearing thick (> 1.5 μ m-thick) electrodeposited Co-oxides on their surfaces evinced photocurrent to O₂ conversion efficiencies of ~100%, and much better stability under operation on account of the much reduced production of peroxy species. Moreover, the onset for O₂ production was shifted cathodically by 170 mV compared to bare WO₃ films.

Meanwhile, Nocera and co-workers reported their own light-harvesting array functionalized with electrodeposited Co-oxides.⁹⁹ In this case, *np*-Si junctions were the light-absorbers chosen, onto which a protective indium-tin oxide (ITO) layer was deposited by sputtering. CoPi was then electrodeposited on this ITO layer, producing an *npp*⁺Si|ITO|Co-Pi photoanode. Irradiation of this photoanode with simulated sunlight (“1 Sun”) in the presence of an applied bias allowed water oxidation to O₂ to proceed at 1 mA cm⁻² at 800 mV lower potential than that required by the same electrodes in the dark. This work was subsequently significantly expanded to produce a monolithic device (an “Artificial Leaf”) in which a buried triple-junction silicon photovoltaic (which therefore produced a greater potential difference under illumination than the less complex devices discussed above) was inserted between two electrodeposited catalyst films (Figure 11).¹⁰⁰ On the anode side, the catalyst chosen was CoPi, whilst on the cathode side the catalyst for the HER was a novel ternary NiMoZn material (which was itself electrodeposited onto the cathode from a solution of the simple metal salts). Irradiation of this device in potassium borate buffer at pH 9.2 allowed simultaneous water oxidation to O₂ and proton reduction to H₂ to be achieved without the need for any



external electrical bias, with a 2.5% solar-to-hydrogen conversion efficiency at 1 Sun illumination.

Fig. 11 Nocera's monolithic artificial leaf. The path of the protons through the electrolyte surrounding the device (which completes the electrical circuit) is shown with the dashed arrows.

BiVO_4 and titania have also been used as substrates for Co-oxide electrodeposition. In the former case, van de Krol and co-workers decorated BiVO_4 with thin CoPi-like catalysts by electrodeposition.¹⁰¹ Film thicknesses of 30 nm were found to present a good balance between the competing demands of catalyst efficiency and film transparency. Under simulated sunlight, currents of 1.7 mA cm^{-2} were obtained at biases of 1.23 V vs. RHE. In subsequent work, van de Krol was able to improve this performance and achieve 2.3 mA cm^{-2} at 1.23 V vs. RHE by doping the BiVO_4 substrates with 1% tungsten before electrodepositing CoPi on top as before.¹⁰² Herring and co-workers have also investigated BiVO_4 -derived materials as substrates for CoPi electrodeposition.¹⁰³ These authors first prepared porous SiO_2 - BiVO_4 electrodes by a modification of a previously reported metal-organic decomposition procedure,¹⁰⁴ and then CoPi was electrodeposited onto this substrate. When compared to the performance of films that had been produced by photo-assisted electrodeposition at 1 Sun under otherwise identical conditions, photo-electrodeposited catalysts were found to give significantly enhanced photocurrents relative to purely electrodeposited films. This enhanced performance of photo-electrodeposited films was attributed to more uniform distribution of the catalyst across the surface of the semiconductor, in a similar manner to that previously reported by Gamelin.⁹⁵⁻⁹⁷

Table 6: Key data for the electrodeposited catalysts for photo-driven water oxidation discussed in Section 8.

Reference	Catalytic Oxide	Operating pH	Photo-active substrate	Potential to reach 1 mA cm^{-2} at 1 Sun illumination (V vs. RHE)
95	Co	13.6	$\alpha\text{-Fe}_2\text{O}_3$	1.45
96	Co	7 - 13.6	$\alpha\text{-Fe}_2\text{O}_3$	1.1
97	Co	13.6	$\alpha\text{-Fe}_2\text{O}_3$	1
98	Co	7	WO_3	1.2^a
99	Co	7	$npp^+\text{Si} \text{ITO}$	1.2
100	Co	7	3jn-Si	No external bias
101	Co	5.6	BiVO_4	1
102	Co	5.6	W-doped BiVO_4	1
103	Co	7	BiVO_4	1.2
105	Co	7	TiO_2	1.7^b
106	Co	6.8	$\text{TiO}_2\text{-}g\text{C}_3\text{N}_4$	1
107	Ni	9.2	BiVO_4	1
108	Ni	7	W-doped BiVO_4	1.3
109	Ni	9.2	WO_3	1.2
110	NiFe	14	Ti-doped $\alpha\text{-Fe}_2\text{O}_3$	1.1^c
111	Fe	14	$\alpha\text{-Fe}_2\text{O}_3$ (the oxide itself)	1.1

^a Current density is 0.5 mA cm^{-2} at this potential. ^b Current density is 0.4 mA cm^{-2} at this potential and light source is broad band 200 mW cm^{-2} . ^c Light intensity not specified.

Khayzer *et al.* decorated a TiO_2 -on-FTO electrode with a CoPi-like catalyst at pH 7 by using the TiO_2 -FTO electrode as the anode in a 2-electrode photoelectrochemical cell (with a Pt counter electrode).

Irradiation of the anode with UV light ($\lambda_{\text{ex}} = 365 \text{ nm}$) for 15 hours was sufficient to cause CoPi to electrodeposit on the surface of the TiO_2 , without the need for any additional bias.¹⁰⁵ These films were compared to those obtained by direct electrodeposition of CoPi onto TiO_2 -FTO supports in the dark at 1.1 V vs. Ag/AgCl. The structures and activities of the two types of electrode were found to be similar, confirming that CoPi could be deposited on TiO_2 substrates in a photoelectrochemical cell without the application of an external bias without any loss in activity compared to purely electrodeposited materials. Recently, Li and co-workers have demonstrated that CoPi can be electrodeposited on hybrid TiO_2 - $g\text{C}_3\text{N}_4$ substrates (where $g\text{C}_3\text{N}_4$ is graphitic carbon nitride) from solutions containing 0.15 mM cobalt nitrate at pH 7 and at 1.1 V vs. Ag/AgCl.¹⁰⁶ The photocatalytic performance of these electrodes for the OER under 1 Sun was found to be about 30% better (at a bias of +1.5 V vs. RHE) than that of undecorated TiO_2 - $g\text{C}_3\text{N}_4$ substrates, which in turn showed about 3 times the activity of TiO_2 under the same conditions.

Ni-oxide electrodeposits have also been generated on semiconductor substrates for use as photoanodes for the OER. Park and co-workers undertook the electrodeposition of NiBi on BiVO_4 substrates from borate solutions containing 1 mM Ni^{2+} at potentials of +1.2 V vs. SCE.¹⁰⁷ The performance of these films was then compared to that obtained from the same set-up, but where the required potential bias for deposition was supplied solely by irradiation of the BiVO_4 substrate (an intensity of ~ 4 Suns was used). Both dark-electrodeposited and photo-electrodeposited films were optimized to a thickness of around 40 nm. Photo-electrodeposited films performed marginally better as catalysts for the OER than those electrodeposited in the dark, in line with similar experiments performed with Co (see above). In both cases, however, catalysis was several times more effective than with bare BiVO_4 . The authors attributed this increased OER activity in the presence of NiBi to enhanced hole transfer from BiVO_4 to water mediated by the Ni-oxide film, with the result that NiBi can be viewed as facilitating the generation of long-lived holes. Pilli *et al.* have also electrodeposited nickel oxides on BiVO_4 substrates, in this case using W-doped BiVO_4 as the semiconductor.¹⁰⁸ Under illumination at 1 Sun, films decorated with these Ni-oxides achieved current densities for the OER of 1 mA cm^{-2} at 600 mV lower overpotential than for bare W-doped BiVO_4 .

Tungsten oxides have also been used in their own right as substrates for Ni-oxide electrodepositions. An example of this was reported by Diao and co-workers, who formed NiBi on the surface of WO_3 "nanoneedles" by a photo-assisted electrodeposition technique. This involved applying a bias potential of +1 V vs. SCE to the WO_3 anodes in a borate electrolyte (pH 9.2) containing 1 mM nickel acetate, whilst simultaneously irradiating the electrode with a Xe lamp at an intensity of 120 mW cm^{-2} . These functionalised electrodes produced roughly twice as much oxygen per unit time under anodic bias when compared to bare WO_3 and exhibited solar-to-hydrogen conversion efficiencies of around 1.7%.¹⁰⁹

McFarland and co-workers have electrodeposited various NiFe-oxides on Ti-doped hematite electrodes and have assessed the performance of these as photoanodes for the OER at pH 14.¹¹⁰ NiSO_4 was used as the nickel source, but two different iron sources were employed: Fe(II) sulfate and Fe(III) sulfate. Electrodeposition

onto the Ti-hematite substrates was then performed using a square pulse method: -1.2 V vs. Ag/AgCl was applied for $50 \mu\text{s}$, followed by a pulse at -0.5 V vs. Ag/AgCl for $50 \mu\text{s}$. Catalysts deposited in this manner from Ni(II) and Fe(II) precursors displayed the highest activity for the OER when run under purely electrochemical conditions (in the dark), but catalysts deposited from mixtures of Ni(II) and Fe(III) precursors displayed the highest activity for the OER under photo-electrochemical conditions. These differences in performance are perhaps linked to different metal oxidation states and stoichiometries within the films: XPS indicated that both Ni(II)/Fe(II) and Ni(II)/Fe(III) films contained Fe^{3+} but those deposited from Ni(II)/Fe(II) also contained observable amounts of Fe^0 and Ni^0 . Moreover, the two types of film had very different Fe-contents: Ni(II)/Fe(II)-derived films contained 41% atomic% Fe (calculated by $\text{Fe}/(\text{Fe}+\text{Ni})$), whereas for Ni(II)/Fe(III)-derived films this figure was closer to 95%.

Finally, we noted that iron-only oxide films for the photo-assisted OER have been reported by Zhou and co-workers.¹¹¹ These authors used aqueous solutions of FeSO_4 containing ammonia at pH 10.8 as their deposition baths. After deposition, the films were annealed in air, with an annealing temperature of 500°C found to be optimal. These films were found to deliver the highest currents for water oxidation yet reported by undoped $\alpha\text{-Fe}_2\text{O}_3$.

9. Conclusions and outlook

In this review, we have given an overview of electrodeposited catalysts for the OER that are based on first row transition metals, with a special emphasis on more recent examples that are of relevance to potential solar-driven water splitting. With regards to this over-arching goal, systems that use neutral or near-neutral electrolytes are probably the most promising for potential applications, as the less corrosive nature of these electrolytes will reduce the burden on cell components, not the least important of which are the photoactive semiconductor substrates and the water splitting electrocatalysts themselves. Moreover, when deployed over the large areas required to obtain useful amounts of hydrogen on reasonable timescales, less corrosive electrolytes will have key advantages in terms of safety and the regulation that will inevitably follow the development of any mass-produced (or mass-producible) device. That said, harsher conditions (more acidic or basic electrolytes, additives, higher temperatures) may well find utility in higher current density point-source electrolyser (*e.g.* running off photovoltaic panels external to the electrolyser itself) or in particular specialised applications. Regardless of the path to device development that is eventually followed, it seems that electrochemical water splitting will continue to be a very active field of research for many years to come, not least because the oxygen evolution reaction remains such a demanding process to perform. Electrodeposition is a relatively inexpensive technique, and affords a ready route by which to control catalyst thickness, morphology and oxidation state. It is likely therefore that many more papers reporting electrodeposited catalysts for water oxidation will appear in the coming years. We hope that this review will go some way towards educating the next

generation of scientists as they advance this challenging and fascinating field.

Acknowledgements

MDS thanks the University of Glasgow for a Kelvin-Smith Research Fellowship. We acknowledge Asst. Prof. Yogesh Surendranath (Massachusetts Institute of Technology) for supplying parts of Figure 1.

References

- N. S. Lewis and D. G. Nocera, *Proc. Natl. Acad. Sci. USA*, 2006, **103**, 15729.
- S. Dasgupta, B. S. Brunschwig, J. R. Winkler and H. B. Gray, *Chem. Soc. Rev.* 2013, **42**, 2213.
- Y. Tachibana, L. Vayssieres and J. R. Durrant, *Nat. Photonics*, 2012, **6**, 511.
- T. R. Cook, D. K. Dogutan, S. Y. Reece, Y. Surendranath, T. S. Teets and D. G. Nocera, *Chem. Rev.* 2010, **110**, 6474.
- B. Rausch, M. D. Symes, G. Chisholm and L. Cronin, *Science*, 2014, **345**, 1326.
- R. E. Blankenship, D. M. Tiede, J. Barber, G. W. Brudvig, G. Fleming, M. Ghirardi, M. R. Gunner, W. Junge, D. M. Kramer, A. Melis, T. A. Moore, C. C. Moser, D. G. Nocera, A. J. Nozik, D. R. Ort, W. W. Parson, R. C. Prince and R. T. Sayre, *Science*, 2011, **332**, 805.
- M. Carmo, D. L. Fritz, J. Mergel and D. Stolten, *Int. J. Hydrogen Energy*, 2013, **38**, 4901.
- M. G. Walter, E. L. Warren, J. R. McKone, S. W. Boettcher, Q. Mi, E. A. Santori and N. S. Lewis, *Chem. Rev.* 2010, **110**, 6446.
- C. C. L. McCrory, S. Jung, J. C. Peters and T. F. Jaramillo, *J. Am. Chem. Soc.* 2013, **135**, 16977.
- C. C. L. McCrory, S. Jung, I. M. Ferrer, S. M. Chatman, J. C. Peters and T. F. Jaramillo, *J. Am. Chem. Soc.* 2015, **137**, 4347.
- U.S Department of the Interior, U.S. Geological Survey Mineral Commodities Survey 2015, <http://minerals.usgs.gov/minerals/pubs/mcs/2015/mcs2015.pdf> (accessed November 2015).
- C. L. Fan and D. L. Piron, *Surf. Coat. Technol.* 1995, **73**, 91.
- I. M. Dharmadasa and J. Haigh, *J. Electrochem. Soc.* 2006, **153**, G47.
- G. H. A. Therese and P. V. Kamath, *Chem. Mater.* 2000, **12**, 1195.
- K.-S. Choi, H. S. Jang, C. M. McShane, C. G. Read and J. A. Seabold, *MRS Bull.* 2010, **35**, 753.
- M. W. Kanan and D. G. Nocera, *Science*, 2008, **321**, 1072.
- D. A. Lutterman, Y. Surendranath and D. G. Nocera, *J. Am. Chem. Soc.* 2009, **131**, 3838.
- M. Risch, V. Khare, I. Zaharieva, L. Gerencser, P. Chernev and H. Dau, *J. Am. Chem. Soc.* 2009, **131**, 6936.
- M. W. Kanan, J. Yano, Y. Surendranath, M. Dincă, V. K. Yachandra and D. G. Nocera, *J. Am. Chem. Soc.* 2010, **132**, 13692.
- A. J. Esswein, Y. Surendranath, S. Y. Reece and D. G. Nocera, *Energy Environ. Sci.* 2011, **4**, 499.
- J. G. McAlpin, Y. Surendranath, M. Dincă, T. A. Stich, S. A. Stoian, W. H. Casey, D. G. Nocera and R. D. Britt, *J. Am. Chem. Soc.* 2010, **132**, 6882.
- Y. Surendranath, M. W. Kanan and D. G. Nocera, *J. Am. Chem. Soc.* 2010, **132**, 16501.
- Y. Surendranath, M. Dincă and D. G. Nocera, *J. Am. Chem. Soc.* 2009, **131**, 2615.
- C. L. Farrow, D. K. Bediako, Y. Surendranath, D. G. Nocera and S. J. L. Billinge, *J. Am. Chem. Soc.*, 2013, **135**, 6403.
- Y. Lee, J. Suntivich, K. J. May, E. E. Perry, and Y. Shao-Horn, *J. Phys. Chem. Lett.* 2012, **3**, 399.
- S. Cobo, J. Heidkamp, P.-A. Jacques, J. Fize, V. Fourmond, L. Guetaz, B. Jousselme, V. Ivanova, H. Dau, S. Palacin, M. Fontecave and V. Artero, *Nature Mater.* 2012, **11**, 802.
- J. B. Gerken, E. C. Landis, R. J. Hamers and S. S. Stahl, *ChemSusChem*, 2010, **3**, 1176.
- J. B. Gerken, J. G. McAlpin, J. Y. C. Chen, M. L. Rigsby, W. H. Casey, R. D. Britt and S. S. Stahl, *J. Am. Chem. Soc.* 2011, **133**, 14431.
- L. G. Bloor, P. I. Molina, M. D. Symes and L. Cronin, *J. Am. Chem. Soc.* 2014, **136**, 3304.
- J. A. Koza, Z. He, A. S. Miller and J. A. Switzer, *Chem. Mater.* 2012, **24**, 3567.
- J. Zhu, F. Lambert, C. Policar, F. Mavré and B. Limoges, *J. Mater. Chem. A*, 2015, **3**, 16190.
- N. Jiang, B. You, M. Sheng and Y. Sun, *Angew. Chem. Int. Ed.* 2015, **54**, 6251.
- J. J. Stracke and R. G. Finke, *J. Am. Chem. Soc.* 2011, **133**, 14872.
- J. J. Stracke and R. G. Finke, *ACS Catal.* 2013, **3**, 1209.
- Y.-H. Lai, C.-Y. Lin, Y. Lv, T. C. King, A. Steiner, N. M. Muresan, L. Gan, D. S. Wright and E. Reisner, *Chem. Commun.* 2013, **49**, 4331.
- Y. Liu, S.-X. Guo, L. Ding, C. A. Ohlin, A. M. Bond and J. Zhang, *ACS Appl. Mater. Interfaces*, 2015, **7**, 16632.
- H. Chen, Z. Sun, X. Liu, A. Han and P. Du, *J. Phys. Chem. C*, 2015, **119**, 8998.
- A. Han, H. Wu, Z. Sun, H. Jia, Z. Yan, H. Ma, X. Liu and P. Du, *ACS Appl. Mater. Interfaces*, 2014, **6**, 10929.
- A. M. Ullman, Y. Liu, M. Huynh, D. K. Bediako, H. Wang, B. L. Anderson, D. C. Powers, J. J. Breen, H. D. Abruña and D. G. Nocera, *J. Am. Chem. Soc.* 2014, **136**, 17681.
- S. A. Bonke, M. Wiechen, R. K. Hocking, X.-Y. Fang, D. W. Lupton, D. R. MacFarlane and L. Spiccia, *ChemSusChem*, 2015, **8**, 1394.
- M. Dincă, Y. Surendranath and D. G. Nocera, *Proc. Natl. Acad. Sci. USA*, 2010, **107**, 10337.
- D. K. Bediako, Y. Surendranath and D. G. Nocera, *J. Am. Chem. Soc.* 2013, **135**, 3662.
- D. K. Bediako, B. Lassalle-Kaiser, Y. Surendranath, J. Yano, V. K. Yachandra and D. G. Nocera, *J. Am. Chem. Soc.* 2012, **134**, 6801.
- M. Risch, K. Klingan, J. Heidkamp, D. Ehrenberg, P. Chernev, I. Zaharieva and H. Dau, *Chem. Commun.* 2011, **47**, 11912.
- Z. Chen, A. R. Rathmell, S. Ye, A. R. Wilson and B. J. Wiley, *Angew. Chem. Int. Ed.* 2013, **52**, 13708.
- L.-K. Wu, J.-M. Hu, J.-Q. Zhang and C.-N. Cao, *J. Mater. Chem. A*, 2013, **1**, 12885.
- C. He, X. Wu and Z. He, *J. Phys. Chem. C*, 2014, **118**, 4578.
- X. Yu, T. Hua, X. Liu, Z. Yan, P. Xu and P. Du, *ACS Appl. Mater. Interfaces*, 2014, **6**, 15395.
- A. Singh, S. L. Y. Chang, R. K. Hocking, U. Bach and L. Spiccia, *Energy Environ. Sci.* 2013, **6**, 579.
- A. Singh, S. L. Y. Chang, R. K. Hocking, U. Bach and L. Spiccia, *Catal. Sci. Technol.* 2013, **3**, 1725.
- I. Roger and M. D. Symes, *J. Am. Chem. Soc.* 2015, **137**, 13980.
- J. A. Widegren and R. G. Finke, *J. Mol. Catal. A: Chem.* 2003, **198**, 317.
- R. H. Crabtree, *Chem. Rev.* 2012, **112**, 1536.
- J. Barber, *Inorg. Chem.* 2008, **47**, 1700.
- S. Trasatti, *Electrochim. Acta*, 1984, **29**, 1503.
- M. Morita, C. Iwakura and H. Tamura, *Electrochim. Acta*, 1979, **24**, 357.
- Y. Gorlin and T. F. Jaramillo, *J. Am. Chem. Soc.* 2010, **132**, 13612.
- Y. Gorlin, B. Lassalle-Kaiser, J. D. Benck, S. Gul, S. M. Webb, V. K. Yachandra, J. Yano and T. F. Jaramillo, *J. Am. Chem. Soc.* 2013, **135**, 8525.
- B. A. Pinaud, Z. Chen, D. N. Abram and T. F. Jaramillo, *J. Phys. Chem. C*, 2011, **115**, 11830.
- T. Takashima, K. Hashimoto and R. Nakamura, *J. Am. Chem. Soc.* 2012, **134**, 1519.
- T. Takashima, K. Hashimoto and R. Nakamura, *J. Am. Chem. Soc.* 2012, **134**, 18153.
- I. Zaharieva, P. Chernev, M. Risch, K. Klingan, M. Kohlhoff, A. Fischer and H. Dau, *Energy Environ. Sci.* 2012, **5**, 7081.
- G. Mattioli, I. Zaharieva, H. Dau and L. Guidoni, *J. Am. Chem. Soc.* 2015, **137**, 10254.
- A. Ramírez, P. Hillebrand, D. Stellmach, M. M. May, P. Bogdanoff and S. Fiechter, *J. Phys. Chem. C*, 2014, **118**, 14073.
- F. Zhou, A. Izgorodin, R. K. Hocking, V. Armel, L. Spiccia and D. R. MacFarlane, *ChemSusChem*, 2013, **6**, 643.

- 66 F. Zhou, A. Izgorodin, R. K. Hocking, L. Spiccia and D. R. MacFarlane, *Adv. Energy Mater.* 2012, **2**, 1013.
- 67 W. T. Osowiecki, S. W. Sheehan, K. J. Young, A. C. Durrell, B. Q. Mercado and G. W. Brudvig, *Dalton Trans.* 2015, **44**, 16873.
- 68 M. Huynh, D. K. Bediako, Y. Liu and D. G. Nocera, *J. Phys. Chem. C*, 2014, **118**, 17142.
- 69 M. Huynh, D. K. Bediako and D. G. Nocera, *J. Am. Chem. Soc.* 2014, **136**, 6002.
- 70 Z. Chen and T. J. Meyer, *Angew. Chem. Int. Ed.* 2013, **52**, 700.
- 71 F. Yu, F. Li, B. Zhang, H. Li and L. Sun, *ACS Catal.* 2015, **5**, 627.
- 72 X. Liu, H. Jia, Z. Sun, H. Chen, P. Xu and P. Du, *Electrochem. Commun.* 2014, **46**, 1.
- 73 T.-T. Li, S. Cao, C. Yang, Y. Chen, X.-J. Lv and W.-F. Fu, *Inorg. Chem.* 2015, **54**, 3061.
- 74 X. Liu, H. Zheng, Z. Sun, A. Han and P. Du, *ACS Catal.* 2015, **5**, 1530.
- 75 Y. Wu, M. Chen, Y. Han, H. Luo, X. Su, M.-T. Zhang, X. Lin, J. Sun, L. Wang, L. Deng, W. Zhang and R. Cao, *Angew. Chem. Int. Ed.* 2015, **54**, 4870.
- 76 M. Chen, Y. Wu, Y. Han, X. Lin, J. Sun, W. Zhang and R. Cao, *ACS Appl. Mater. Interfaces*, 2015, **7**, 21852.
- 77 D. A. Corrigan, *J. Electrochem. Soc.* 1987, **134**, 377.
- 78 M. D. Merrill and R. C. Dougherty, *J. Phys. Chem. C*, 2008, **112**, 3655.
- 79 X. Li, F. C. Walsh and D. Pletcher, *Phys. Chem. Chem. Phys.* 2011, **13**, 1162.
- 80 X. Lu and C. Zhao, *Nat. Commun.* 2015, **6**, 6616.
- 81 M. W. Louie and A. T. Bell, *J. Am. Chem. Soc.* 2013, **135**, 12329.
- 82 D. Friebel, M. W. Louie, M. Bajdich, K. E. Sanwald, Y. Cai, A. M. Wise, M.-J. Cheng, D. Sokaras, T.-C. Weng, R. Alonso-Mori, R. C. Davis, J. R. Bargar, J. K. Nørskov, A. Nilsson and A. T. Bell, *J. Am. Chem. Soc.* 2015, **137**, 1305.
- 83 L. Trotochaud, S. L. Young, J. K. Ranney and S. W. Boettcher, *J. Am. Chem. Soc.* 2014, **136**, 6744.
- 84 D. A. Corrigan, R. S. Conell, C. A. Fierro and D. A. Scherson, *J. Phys. Chem.* 1987, **91**, 5009.
- 85 A. M. Smith, L. Trotochaud, M. S. Burke and S. W. Boettcher, *Chem. Commun.* 2015, **51**, 5261.
- 86 D. Wang, J. Zhou, Y. Hu, J. Yang, N. Han, Y. Li and T.-K. Sham, *J. Phys. Chem. C*, 2015, **119**, 19573.
- 87 M. Gong, Y. Li, H. Wang, Y. Liang, J. Z. Wu, J. Zhou, J. Wang, T. Regier, F. Wei and H. Dai, *J. Am. Chem. Soc.* 2013, **135**, 8452.
- 88 M. S. Burke, M. G. Kast, L. Trotochaud, A. M. Smith and S. W. Boettcher, *J. Am. Chem. Soc.* 2015, **137**, 3638.
- 89 T. N. Lambert, J. A. Vigil, S. E. White, D. J. Davis, S. J. Limmer, P. D. Burton, E. N. Coker, T. E. Beechem and M. T. Brumbach, *Chem. Commun.* 2015, **51**, 9511.
- 90 J. Tian, N. Cheng, Q. Liu, X. Sun, Y. He and A. M. Asiri, *J. Mater. Chem. A*, 2015, **3**, 20056.
- 91 Y. Li, L. Zhang, X. Xiang, D. Yan and F. Li, *J. Mater. Chem. A*, 2014, **2**, 13250.
- 92 X. Li, G. Guan, X. Du, J. Cao, X. Hao, X. Ma, A. D. Jagdale and A. Abudula, *Chem. Commun.* 2015, **51**, 15012.
- 93 X. Hao, T. Yan, Z. Wang, S. Liu, Z. Liang, Y. Shen and M. Pritzker, *Thin Solid Films*, 2012, **520**, 2438.
- 94 J. A. Haber, Y. Cai, S. Jung, C. Xiang, S. Mitrovic, J. Jin, A. T. Bell and J. M. Gregoire, *Energy Environ. Sci.* 2014, **7**, 682.
- 95 D. K. Zhong, J. Sun, H. Inumaru and D. R. Gamelin, *J. Am. Chem. Soc.* 2009, **131**, 6086.
- 96 D. K. Zhong and D. R. Gamelin, *J. Am. Chem. Soc.* 2010, **132**, 4203.
- 97 D. K. Zhong, M. Cornuz, K. Sivula, M. Grätzel and D. R. Gamelin, *Energy Environ. Sci.* 2011, **4**, 1759.
- 98 J. A. Seabold and K.-S. Choi, *Chem. Mater.* 2011, **23**, 1105.
- 99 J. J. H. Pijpers, M. T. Winkler, Y. Surendranath, T. Buonassisi and D. G. Nocera, *Proc. Natl. Acad. Sci. USA*, 2011, **108**, 10056.
- 100 S. Y. Reece, J. A. Hamel, K. Sung, T. D. Jarvi, A. J. Esswein, J. J. H. Pijpers and D. G. Nocera, *Science*, 2011, **334**, 645.
- 101 F. F. Abdi and R. van de Krol, *J. Phys. Chem. C*, 2012, **116**, 9398.
- 102 F. F. Abdi, N. Firet and R. van de Krol, *ChemCatChem*, 2013, **5**, 490.
- 103 S. K. Pilli, T. G. Deutsch, T. E. Furtak, J. A. Turner, L. D. Brown and A. M. Herring, *Phys. Chem. Chem. Phys.* 2012, **14**, 7032.
- 104 A. Galembeck and O. L. Alves, *Thin Solid Films*, 2000, **365**, 90.
- 105 R. S. Khayzer, M. W. Mara, J. Huang, M. L. Shelby, L. X. Chen and F. N. Castellano, *ACS Catal.* 2012, **2**, 2150.
- 106 Y. Li, R. Wang, H. Li, X. Wei, J. Feng, K. Liu, Y. Dang and A. Zhou, *J. Phys. Chem. C*, 2015, **119**, 20283.
- 107 S. K. Choi, W. Choi and H. Park, *Phys. Chem. Chem. Phys.* 2013, **15**, 6499.
- 108 S. K. Pilli, K. Summers and D. Chidambaram, *RSC Adv.* 2015, **5**, 47080.
- 109 T. Jin, P. Diao, D. Xu and Q. Wu, *Electrochim. Acta*, 2013, **114**, 271.
- 110 A. Kleiman-Shwarsstein, Y.-S. Hu, G. D. Stucky and E. W. McFarland, *Electrochem. Commun.* 2009, **11**, 1150.
- 111 Q. Zeng, J. Bai, J. Li, L. Xia, K. Huang, X. Li and B. Zhou, *J. Mater. Chem. A*, 2015, **3**, 4345.